Available online at www.sciencedirect.com
ScienceDirect
Journal of Power Sources 159 (2006) 340–344
JOURNAL OF POWER SOURCES
www.elsevier.com/locate/jpowsour

Short communication

Anodic properties of tin oxides with pyrochlore structure for lithium ion batteries

N. Sharma, G.V. Subba Rao, B.V.R. Chowdari *

Department of Physics, National University of Singapore, Singapore 117542, Singapore

Available online 6 June 2006

Abstract

Mixed tin oxides, $M_2Sn_2O_7$ (M = Y, Nd), with cubic pyrochlore structure were synthesized and characterized by X-ray diffraction and SEM. Galvanostatic cycling versus Li metal in the voltage range, 0.005–1.0 V at the current density of 60 mA g^{-1} showed that the first-discharge capacities are 913 and 722 mA hg^{-1} whereas the first-charge capacities are 350 and 265 (±3) mA hg^{-1}, for M = Y and Nd, respectively. The corresponding number of moles of recyclable Li are 3.4 and 3.2 for M = Y and Nd. Crystal structure destruction occurs during the first-discharge leading to the formation of nano-particles of Sn-metal and finally $Li_{4.4}Sn$ in a matrix of Li–M–O. After 50 cycles, both compounds showed a capacity-retention of 89 (±1)% of the 10th cycle reversible capacity. The coulombic efficiency is ∼98%. The average charge and discharge voltages in both compounds are 0.5 and 0.25 V, respectively. Cyclic voltammograms complement the galvanostatic results and showed that a good operating voltage range is 0.005–1.0 V. The electrodic performances of $M_2Sn_2O_7$ have been compared with those exhibited by other crystalline ternary tin oxides.

Keywords: Tin oxides; Pyrochlores; Electrochemical properties; Li-ion batteries

1. Introduction

Binary and ternary tin (Sn) oxides have been extensively investigated as anode materials for lithium ion batteries (LIB) [1–9]. This is attributable to the large reversible capacity and good operable voltage range, 0.25–0.5 V versus Li metal in comparison to the presently used graphite anode in LIB. The electrochemical cycling takes place via Li_xSn alloy formation up on deep discharge and the 'Sn' metal formation during the charge reaction. Major problem posed by tin oxides is the large volume variations that occur during alloying–dealloying reactions leading to instabilities in the electrode and its failure [1]. Several strategies have been employed to overcome this problem: (i) incorporating Sn-metal or ions in a suitable metal/non-metal matrix that can buffer the volume changes [2,4,5,8,9], (ii) reducing the particle size [1,7,8] and (iii) choosing appropriate voltage range of operation [3,5,7–9]. Based on these measures, a large number and wide variety of crystalline/amorphous/glassy/nano-phase tin compounds have been examined [2–9]. As a result, it is established that the starting crystal structure of the Sn-compound, SnO_y coordination polyhedron and the matrix (M) metal/non-metal ions play an important role in governing the large and stable reversible capacities. Even though the crystal structure of the compound gets destroyed during the first-discharge reaction with Li, it should still strongly influence the local structure of the resulting non-crystalline or nano-crystalline lithiated material, Li–M–O along with the Sn and Li_xSn nano-particles and affect the electrochemistry of Li-de-insertion/insertion [5,8,9].

Mixed tin oxides with inverse spinel [6], perovskite [8], cubic network [5] and hollandite [9] crystal structure have been studied for their Li-recyclability. Ternary tin oxides with the cubic pyrochlore structure, $M_2Sn_2O_7$, M = rare earth or yttrium (Y) constitute a well-known series of compounds possessing SnO_6 octahedra [10,11]. The pyrochlore structure can be derived from the fluorite (CaF_2) structure and the M-ions adapt an eight-fold O-coordination. It will be of interest to examine the electrochemical behavior of the tin-pyrochlore oxides towards Li metal and to find out their applicability as anodes for LIB. We carried out studies on $M_2Sn_2O_7$ (M = Y, Nd) and the results are reported. The electrochemical cycling results of these are compared with those of other tin oxides described in literature.

2. Experimental

The compounds $Y_2Sn_2O_7$ and $Nd_2Sn_2O_7$ were synthesized by heating the pellets of ground stoichiometric mixture of

* Corresponding author. Tel.: +65 6874 2956; fax: +65 6777 6126.
E-mail address: phychowd@nus.edu.sg (B.V.R. Chowdari).

0378-7753/$ – see front matter © 2006 Elsevier B.V. All rights reserved.
doi:10.1016/j.jpowsour.2006.04.050

Y_2O_3/Nd_2O_3 and SnO_2 (all Merck) at 900 °C in air in a box furnace (Carbolite, UK) for 25 h. These were cooled, reground, pelletized and reheated at 1250 °C in air for 24 h, cooled and reground to fine-powder.

X-ray diffraction (XRD) patterns were taken using Siemens D5005 equipped with Cu Kα radiation in 2θ range, 10–80° and lattice parameters were derived by the least squares fitting method. Surface morphology was examined using SEM (JEOL JSM-6700F, Field Emission Electron Microscope). The electrochemical studies were carried out with respect to Li in the form of coin cell using the oxides as cathodes. The electrode fabrication process has been described earlier [8,9]. The composite electrode is made up of a mixture of active material, Super P carbon and binder (Kynar 2801) in the weight ratio, 70:15:15. The thick film (20–30 μm) electrodes were pressed between twin rollers prior to cutting in to circular discs (16 mm). The electrodes were dried at 70 °C for 12 h and then transferred to an Ar-filled glove box, which maintains <1 ppm of H_2O and O_2 (MBraun, Germany). Coin cells (size, 2016) were fabricated in the glove box. Li metal (Kyokuto Metal Co., Japan) foil was used as the counter electrode, Celgard 2502 membrane as the separator and 1 M $LiPF_6$ in ethylene carbonate (EC) and diethyl carbonate (DEC) (1:1 by volume, Merck Selectipur LP40) as the electrolyte. Electrochemical studies were undertaken after ageing the cells for 24 h. The cyclic voltammetry and galvanostatic charge–discharge cycling were carried out at room temperature (RT = 27 °C) by using MacPile II (Biologic, France) unit and Bitrode multiple battery tester (model SCN, Bitrode, USA). Ex situ XRD studies on charged/discharged electrodes have been done by dismantling, after cycling, two duplicate cells in the glove box and separating the test-electrodes from other cell components. These were then washed with DEC and the electrode material was recovered by scraping out from the Cu-foil. The materials were packed on to the XRD sample holders and protected from the atmosphere by covering them with para-film.

3. Results and discussion

3.1. Structure and morphology

The compounds $Y_2Sn_2O_7$ (Y-Sn) and $Nd_2Sn_2O_7$ (Nd-Sn) are white. The XRD patterns shown in Fig. 1 are in agreement with JCPDS databases (file nos. 88-0506 and 87-1220) based on the cubic pyrochlore crystal structure (space group *Fd3m*) [10,11]. The lattice parameters, given in Fig. 1 are in good agreement with those given in JCPDS files. The SEM photographs of the (Y-Sn) and (Nd-Sn) compounds showed that (Y-Sn) is composed of big non-uniform particles (size, 2–10 μm) as compared to the (Nd-Sn) which has aggregates of sub-micron particles.

3.2. Galvanostatic cycling

The first-cycle voltage-capacity profiles of pyrochlores, (Y-Sn) and (Nd-Sn) at the current density of 60 mA g^{-1} are shown in Fig. 2a. The first-discharge reaction commenced cathodically from the open circuit voltage (OCV = 2.7–2.8 V) to 0.005 V whereas the first-charge reaction was continued only up to 1.0 V. The first-discharge profiles comprise two small voltage steps at ∼0.85 and ∼0.75 V, a sloping region up to 0.3–0.4 V followed by a large and flat voltage region at ∼0.28 V for (Y-Sn) and at ∼0.22 V for (Nd-Sn). The voltage step at ∼0.85 V is absent in (Nd-Sn). Thus, almost complete discharge capacity is nested in the large voltage plateau region. The overall first-discharge capacities for (Y-Sn) and (Nd-Sn) are 913 and 722

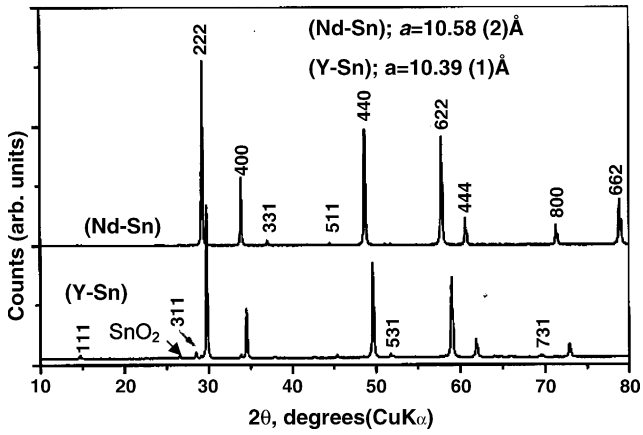

Fig. 1. Powder X-ray diffraction (XRD) patterns of $Y_2Sn_2O_7$ (Y-Sn) and $Nd_2Sn_2O_7$ (Nd-Sn). Cu Kα radiation. Miller indices (h k l) and cubic lattice parameters are shown.

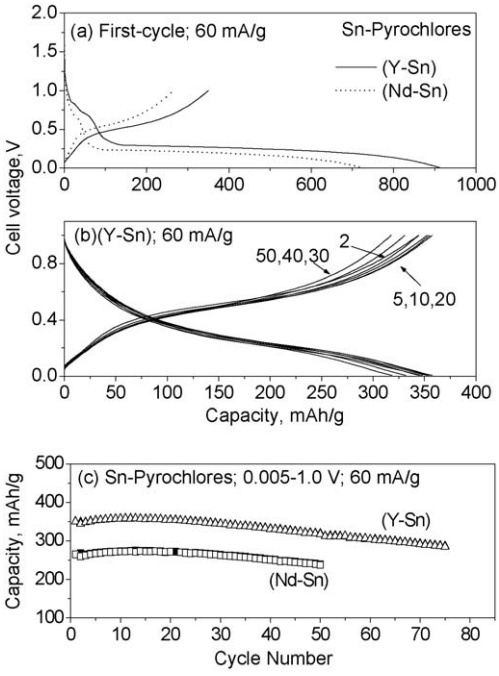

Fig. 2. The voltage vs. capacity profiles for Sn-pyrochlores, $Y_2Sn_2O_7$ (Y-Sn) and $Nd_2Sn_2O_7$ (Nd-Sn). (a) First-discharge–charge cycle from open circuit voltage (OCV = 2.7–2.8 V) to 0.005 V, (b) (Y-Sn), 2–50 cycles in the voltage range, 0.005–1.0 V vs. Li at 60 mA g^{-1}. Only select cycles are shown. Numbers refer to cycle numbers. (c) Capacity vs. cycle number plots for (Y-Sn) (2–75 cycles) and (Nd-Sn) (2–50 cycles), in the voltage range, 0.005–1.0 V. Current density is 60 mA g^{-1}. Filled and open symbols represent discharge and charge capacities, respectively.

(±3) mA hg^{-1}. Based on the molecular weights, these correspond to 18.0 and 17.2 mol of Li consumed in the reaction whereas the theoretical values for both are 16.8 mol of Li as per the Eqs. (1) and (2).

$$M_2Sn_2O_7 + 8Li^+ + 8e^- \rightarrow M_2O_3 + 2Sn + 4Li_2O\,(M = Y, Nd) \quad (1)$$

$$Sn + 4.4Li^+ + 4.4e^- \leftrightarrow Li_{4.4}Sn \quad (2)$$

Analogous to other binary and ternary tin oxides [2–9], the first-discharge reaction involves structure destruction process and the formation of Sn-nano-particles in an amorphous matrix of Y_2O_3 or Nd_2O_3 and Li_2O (Eq. (1)). Due to high M–O bond energies, Li will not reduce M_2O_3 to the respective metals under room temperature electrochemical conditions [12]. Further reaction of Li with Sn-metal results in $Li_{4.4}Sn$ alloy formation (forward reaction of Eq. (2)). Thus, the excess of 1.2 and 0.4 mol of Li consumed by (Y-Sn) and (Nd-Sn), respectively during the first-discharge is ascribed to the formation of solid electrolyte interphase (SEI) on the active material and the passivating layer on the carbon. The small voltage step in the profiles appearing at ~0.75 V may be ascribed to the characteristic passivating layer formation on the carbon used as the additive in the composite electrode [8]. The small voltage plateau at ~0.85 V in (Y-Sn) may be due to slight SnO_2 impurity, detected in the XRD pattern (Fig. 1). The first-discharge voltage profiles for the pyrochlores, (Y-Sn) and (Nd-Sn) (Fig. 2a), resemble those of $ASnO_3$ (A = Ca, Sr, Ba) [8] which possess cubic or distorted cubic perovskite crystal structures and show large voltage plateaus at 0.15–0.3 V versus Li.

The first-charge profiles are smooth with a plateau at ~0.45–0.55 V and show the de-alloying reaction (reverse reaction in Eq. (2)) with the overall capacities, 350 (3.4 mol of Li per Sn) and 265 mA hg^{-1} (3.2 mol of Li/Sn) for (Y-Sn) and (Nd-Sn), respectively (Fig. 2a). The voltage profiles for the subsequent discharge–charge cycles (2–50) for (Y-Sn) are shown in Fig. 2b. Similar to other Sn-oxide systems, the second and subsequent discharge profiles differ from the first-discharge profile. The average discharge and charge potentials are 0.25 and 0.5 V, respectively for both the compounds. The charge and discharge capacities slightly increased from 2–10 cycles, remain almost stable up to 20 cycles but start decreasing slowly afterwards. Similar initial increase in the observed charge–discharge capacities was also noticed in the case of Sn- and other metal-oxides [8,13,14]. This is attributable to the incomplete structure–destruction process that takes place during the first-discharge and continues up to a few initial cycles. The voltage profiles for (Nd-Sn) (2–50 cycles; not shown in Fig. 2) exhibit qualitative similarity to those of (Y-Sn). But the overall-capacity values in the case of (Nd-Sn) are smaller due to the higher atomic weight of Nd, the matrix ion.

Structure destruction of $M_2Sn_2O_7$ compounds upon electrochemical cycling, Li–Sn alloy formation upon deep discharge up to 0.005 V and Sn-metal formation upon charging up to 1.0 V have been corroborated by the ex situ XRD studies on the (Y-Sn) electrode in the discharged- and the charged-state of the 5th cycle (Fig. 3). The peaks corresponding to Li–Sn alloy [15] and Sn-metal [15] are indicated in Fig. 3. The low intensity, broad peaks in the XRD spectra of the discharged electrode are indicative of the crystal structure destruction of the $Y_2Sn_2O_7$ and the formation of nano-Li–Sn alloy. The spectrum comprises peaks due to both Li–Sn alloy and Sn-metal. This may be due to partial decomposition of the alloy while performing the ex situ XRD studies or incomplete formation of the alloy (forward reaction of Eq. (2)). On the other hand, the spectrum of the charged-electrode comprises peaks corresponding to the Sn-metal only.

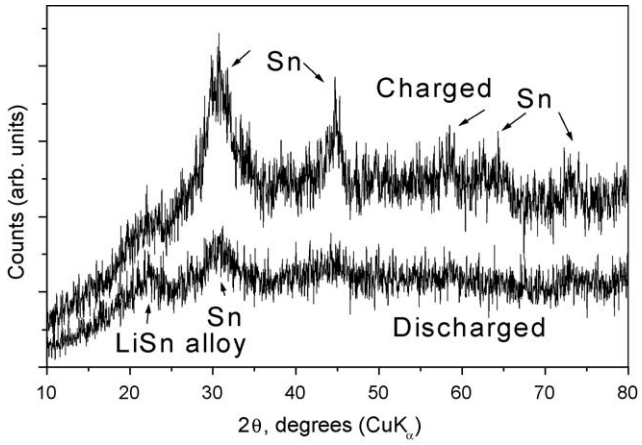

Fig. 3. Ex situ XRD patterns of $Y_2Sn_2O_7$ electrode at the 5th discharge (0.005 V) and charge (1.0 V) cycle. The peaks corresponding to Li–Sn alloy and Sn-metal are indicated.

The capacity versus cycle number plots for the (Y-Sn) up to 75 cycles and (Nd-Sn) up to 50 cycles at a current of 60 mA g^{-1} in the voltage range, 0.005–1.0 V versus Li are shown in Fig. 2c. Qualitatively, the cyclic performance of the two pyrochlores is similar. The 10th cycle capacity values of (Y-Sn) and (Nd-Sn) are 355 (3.5 mol of Li/Sn) and 272 (±3) mA hg^{-1} (3.2 mol of Li/Sn), respectively. The respective capacity-retention values after 50 cycles in both compounds is 89 (±1)% (Fig. 2c). This slow-capacity-fading continues up to 75 cycles in (Y-Sn). The coulombic efficiency is ~98% (Fig. 2b and c).

It is pertinent to compare the cyclic performance of (Y-Sn) and (Nd-Sn) with those of other crystalline Sn-oxides containing SnO_6-octahedra reported in the literature. The 10th cycle reversible capacity of 3.5 and 3.2 mol of cyclable Li/Sn in the above pyrochlores compares well with the values ranging from 3.0–3.4 mol Li/Sn observed in $LiSn_2P_3O_{12}$ and layered-SnP_2O_7 [5], Sn-hollandites, K(M-Sn)O, M = Li, Mg, Fe [9], $CaSnO_3$ [8] and $NaFeSnO_4$ [14], but higher than 2.2–2.4 mol Li/Sn observed in $SrSnO_3$, $BaSnO_3$ and Ca_2SnO_4 [8]. Only cubic-SnP_2O_7 exhibited a 10th cycle reversible capacity value of ~4.0 mol Li/Sn [5]. The capacity-fading, up to 50 cycles and the coulombic efficiency shown by (Y-Sn) and (Nd-Sn) are somewhat similar to those of the above Sn-oxides with the exception of cubic-SnP_2O_7, $CaSnO_3$ and $NaFeSnO_4$. The latter compounds showed almost nil or <5% fading over 50 cycles. Although not examined in this study, it would be interesting to see the rate capability of (Y-Sn) and (Nd-Sn).

3.3. Cyclic voltammetry

The cyclic voltammograms (CV) of (Y-Sn) (voltage, 0.005–2.0 V) and (Nd-Sn) (voltage, 0.005–1.0 V) are shown in Fig. 4a and b. The data were collected at a fairly small sweep rate, 0.058 mV s^{-1}. The Li metal was the counter and reference electrode. First-discharge (cathodic) sweep is devoid of any noticeable peak and current increased rapidly below ∼0.2 V up to the lower cut off voltage limit. This shows that the crystal structure destruction and Li–Sn alloy formation are not taking place at well-defined voltages and the two processes are merging with each other due to close proximity of voltage values involved. Similar behavior was observed in the case of $ASnO_3$ (A = Ca, Sr, Ba) and Ca_2SnO_4 [8]. The first charge-cycle shows a peak at ∼0.6 V in both (Y-Sn) and (Nd-Sn) indicating the de-alloying reaction of $Li_{4.4}Sn$. The CV from the 5th cycle onwards show clear peaks corresponding to various electrode reactions, analogous to those observed for the SnO_6-containing compounds [5,8,9,14]. The CV for (Y-Sn) showed significant decrease in the peak areas under the charge–discharge curves indicative of appreciable capacity-fading when cycled in the voltage range, 0.005–2.0 V as against constant area overlapped-peaks during 5–25 cycles for (Nd-Sn) depicting thereby good cycling response in the voltage range, 0.005–1.0 V. The anodic and cathodic peaks at ∼1.3 and ∼0.9 V, respectively observed in the CV of (Y-Sn) are possibly due to the oxidation/reduction of Sn-metal particles involving Li_2O and matrix as per Eqs. (3a and 3b) [8,14]. The respective peaks at 0.55 and 0.25 V in the CV of both (Y-Sn) and (Nd-Sn) are due to the de-alloying – alloying of Sn, Eq. (2).

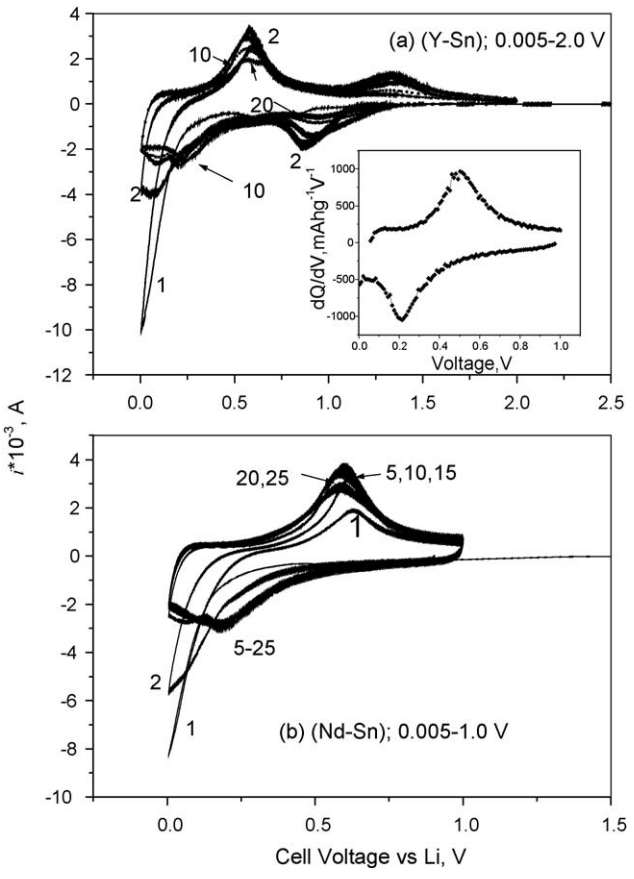

Fig. 4. Cyclic voltammograms of (a) $Y_2Sn_2O_7$ (Y-Sn) in the voltage range 0.005–2.0 V and (b) $Nd_2Sn_2O_7$ (Nd-Sn) in the voltage range 0.005–1.0 V. Li metal was the counter and reference electrode. Scan rate was 0.058 mV s^{-1}. Only select cycles are shown. Numbers refer to cycle numbers. Inset in (a) shows the differential capacity vs. voltage plot of the 10th discharge–charge profile of (Y-Sn) from Fig. 2b.

$$Sn + Li_2O \leftrightarrow SnO + 2Li^+ + 2e^- \quad (3a)$$

$$Sn + 2Li_2O \leftrightarrow SnO_2 + 4Li^+ + 4e^- \quad (3b)$$

The positions of plateau-potentials in the case of galvanostatic cycling are obtained from the differential capacity curve for (Y-Sn) at the 10th cycle (inset of Fig. 4a). The prominent peaks in the differential capacity plot, indicative of well-defined charge and discharge plateau-potentials (∼0.5 and 0.22 V) match with the peak positions of the 10th cycle CV plot shown as dotted line. This shows good agreement between the results obtained via the two different techniques.

4. Conclusions

Tin oxides with the cubic pyrochlore structure $Y_2Sn_2O_7$ (Y-Sn) and $Nd_2Sn_2O_7$ (Nd-Sn) have been investigated as possible anodes for LIB. These contain the electrochemically-active SnO_6 octahedra, and the Y and Nd metals act as the matrix (spectator) ions. The compounds have been synthesized by the high-temperature solid state reaction and characterized by XRD and SEM. Galvanostatic cycling studies were carried out at a current of 60 mA g^{-1} with respect to Li metal in the range, 0.005–1.0 V. The 10th cycle reversible capacities shown by (Y-Sn) and (Nd-Sn) are 350 mA hg^{-1} (3.4 mol Li/Sn) and 265 (±3) mA hg^{-1} (3.2 mol Li/Sn), respectively. Both showed a capacity-retention of 89 (±1)% of the 10th cycle reversible capacity up to 50 cycles. The average charge and discharge voltages were found to be 0.5 and 0.25 V, with coulombic efficiency ∼98% in both the compounds. The CV data complement the galvanostatic cycling results and further indicate that cycling to an upper cut-off voltage of 2.0 V is detrimental to the performance. It may be possible to suppress capacity-fading in (Y-Sn) and (Nd-Sn) by optimizing their particle morphology employing novel low-temperature synthesis methods.

References

[1] M. Winter, J.O. Besenhard, Electrochim. Acta 45 (1999) 31.
[2] Y. Idota, T. Kubota, A. Matsufuji, Y. Maekawa, T. Miyasaka, Science 276 (1997) 1395.
[3] I.A. Courtney, J.R. Dahn, J. Electrochem. Soc. 144 (1997) 2943.
[4] S. Machill, T. Shodai, Y. Sakurai, J. Yamaki, J. Power Sources 73 (1998) 216.
[5] M. Behm, J.T.S. Irvine, Electrochim. Acta 47 (2002) 1727.
[6] P.A. Connor, J.T.S. Irvine, J. Power Sources 97–98 (2001) 223.
[7] D. Aurbach, A. Nimberger, B. Markovsky, E. Levi, E. Sominski, A. Gedanken, Chem. Mater. 14 (2002) 4155.
[8] N. Sharma, K.M. Shaju, G.V. Subba Rao, B.V.R. Chowdari, J. Power Sources 139 (2005) 250.

[9] N. Sharma, J. Plevert, G.V. Subba Rao, B.V.R. Chowdari, T.J. White, Chem. Mater. 17 (2005) 4700.
[10] M.A. Subramanian, G. Aravamudan, G.V. Subba Rao, Progr. Solid. State Chem. 15 (1983) 55.
[11] A.M. Srivastava, Mater. Res. Bull. 37 (2002) 745.
[12] H. Li, P. Balaya, J. Maier, J. Electrochem. Soc. 151 (2004) A1878.
[13] N. Sharma, K.M. Shaju, G.V. Subba Rao, B.V.R. Chowdari, Z.L. Dong, T.J. White, Chem. Mater. 16 (2004) 504.
[14] N. Sharma, K.M. Shaju, G.V. Subba Rao, B.V.R. Chowdari, J. Power Sources 124 (2003) 204.
[15] I.A. Courtney, J.R. Dahn, J. Electrochem. Soc. 144 (1997) 2045.